www.acsnano.org

Spatially Confined Assembly and Immobilization of Hierarchical Nanoparticle Architectures inside Microdroplets in Magnetic Fields

Abhirup Basu, Matthew R. Clary, Joseph B. Tracy, Carol K. Hall, and Orlin D. Velev*



Cite This: ACS Nano 2024, 18, 19814–19827



ACCESS

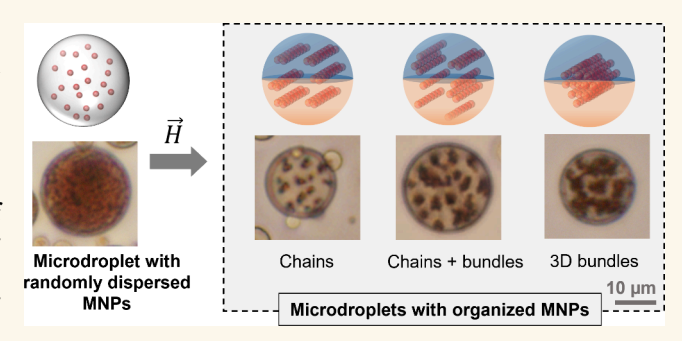
Downloaded via NORTH CAROLINA STATE UNIV on August 6, 2024 at 22:19:34 (UTC). See https://pubs.acs.org/sharingguidelines for options on how to legitimately share published articles.

III Metrics & More

Article Recommendations

Supporting Information

ABSTRACT: Magnetic field-directed colloidal interactions offer facile tools for assembly of structures that range from linear chains to multidimensional hierarchical architectures. While the field-driven assembly of colloidal particles has commonly been investigated in unbounded media, a knowledge gap remains concerning such assembly in confined microenvironments. Here, we investigate how confinement of ferromagnetic nanoparticles in microspheres directs their magnetic assembly into hierarchical architectures. Microdroplets from polydimethylsiloxane (PDMS) liquid precursor containing dispersed iron oxide magnetic nanoparticles (MNPs) were placed in a static magnetic field leading to the



formation of organized assemblies inside the host droplets. By changing the MNP concentrations, we revealed a sequence of microstructures inside the droplets, ranging from linear chains at a low MNP loading, transitioning to a combination of chains and networked bundles, to solely 3D bundles at high MNP loading. These experimental results were analyzed with the aid of COMSOL simulations where we calculated the potential energy to identify the preferred assembly conformations. The chains at high MNP loading minimized their energy by aggregating laterally to form bundles with their MNP dipoles being out-of-registry. We cured these PDMS droplets to immobilize the assemblies by forming soft microbeads. These microbeads constitute an "interaction toolbox" with different magnetic macroscale responses, which are governed by the structuring of the MNPs and their magnetic polarizability. We show that thanks to their ability to rotate by field-induced torque under a rotating field, these microbeads can be employed in applications such as optical modulators and microrollers.

KEYWORDS: microdroplets, magnetic assembly, soft microbeads, hierarchical structures, responsive, magnetic torque, micro rotors

INTRODUCTION

The self-assembly of colloidal particles has emerged as a robust method to fabricate highly ordered structures composed of nanoscale building blocks of different sizes, shapes and compositions. ^{1–4} Such assembled superstructures can help in the creation of advanced functional materials with tunable properties. ^{5–7} The assembly of magnetic particles originates and can be controlled by the dipole—dipole interactions between the particles in a magnetic field. ^{8–10} These interactions are directional in nature and lead to the formation of out-of-equilibrium superstructures, which otherwise would not form in nonmagnetic particle systems. ^{11–13} Field-directed assembly has major advantages in that it is robust and contact-free. This allows the assembly to be controlled from outside the system without the manipulation of the experimental conditions such as

temperature, pH and solvent composition. 14-16 The magnetic dipole—dipole interactions can be attractive or repulsive, based on the angle between the field and the dipoles, imparting significant freedom to the design of experiments.

Colloidal assembly using magnetic fields depends on the interplay between different intrinsic forces including van der Waals and dipole—dipole forces.¹⁷ The magnetic dipolar interactions are usually stronger than the van der Waals forces

Received: May 13, 2024 Revised: July 2, 2024 Accepted: July 5, 2024 Published: July 15, 2024





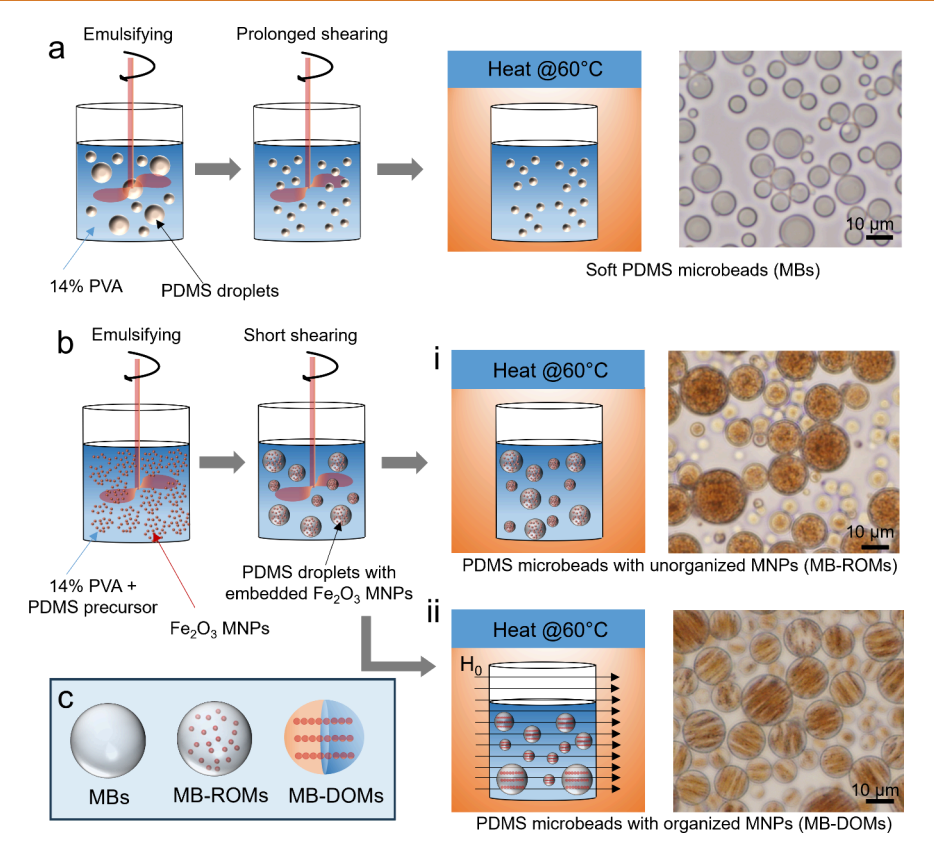


Figure 1. (a) Synthesis of PDMS microbeads by the method of shear-induced droplet breakup in a bulk medium of 14% PVA, and (b) synthesis of PDMS microbeads with embedded MNPs inside the PDMS matrix. The MNPs can be (i) kept randomly dispersed in the absence of a magnetic field (MB-ROMs) or can be (ii) organized into directionally oriented structures (MB-DOMs) in the presence of a uniform magnetic field. (c) Schematics of the structural contents inside each type of microbeads.

and are governed by the magnetic characteristics of the particles such as coercivity, saturation magnetization, and magnetic anisotropy. 18,19 Based on the magnetic energy landscape and the assembly kinetics, the particles can become arrested in kinetically stable states, for example, linear arrangements such as chains, or higher-dimensional structures like sheets and bundles.²⁰⁻²⁴ Additional complexity and precise directionality of the assemblies can be attained by either using colloidal particles that exhibit asymmetry in shape, polarizability and surface properties, or by modulating the field intensity and direction. 25-28 Further, long chains can interact laterally and coalesce in a "zippered' configuration in the presence of toggled fields, and can even form fibrous structures containing bundles of chains.²⁹ One can also attain crystalline superstructures using paramagnetic colloidal particles in the presence of a magnetic field that pulsates on and off at a given frequency. 30,31 Based on the particles' magnetic characteristics, these assembled structures can exhibit different macroscale responses and interactions with and without field. For example, when the field is switched off, the thermal fluctuations can be sufficiently high to overcome the remnant magnetization of the particles and break down the assemblies.³²

One recent advance in this area is the fabrication of composite particles made of a nonmagnetic material such as a hydrogel or elastomer within which magnetic nanoparticle (MNP) assemblies are embedded.^{33–40} Such magnetically responsive composites could find diverse applications such as actuators, microbots, magnetorheological fluids, magnetically controllable colloidal crystals, magnetically controllable colloidal crystals, and biological manipulation. While the assembly behavior of magnetic

nanoparticles in bulk systems or large domains has been reported in multiple studies, ^{20,21,30,31,52,53} an emerging question is how magnetically responsive particles assemble in confined microdomains. In such cases, the patterns formed by the assembled particles not only depend on the strength of the magnetic field, but also on topological constraints such as geometry of the confining environment and the particle packing. 54-56 Normally, in the absence of field interactions, hard particles can transition from a disordered fluid into an ordered crystal or other organized structures due to the spatial confinement. 57,58 In those cases, confinement mediates the entropy effects to determine the final structures of the assemblies. However, in the case of field-mediated assembly, we do not have prior knowledge of the basic process outcome, for example, how change in the size of domain geometry, MNP loading, and field strength can reciprocally affect the structures of the assemblies. Hence, there is a need to elucidate the organization of MNPs within restricted microenvironments that are traversed by magnetic fields.

In this study, we characterized the hierarchical evolution of the microstructural motifs confined inside PDMS microdroplets of various sizes under a uniform magnetic field as the MNP concentration inside is increased. By systematically varying the MNP concentration from 1.25 wt % to 20 wt %, we discovered many structural phases ranging from disconnected short chains to 2D linear chains to 3D networked bundles. We established correlations between the numbers of chains formed inside the host droplets and the cross-sectional area of the droplets. COMSOL simulations were used to evaluate how the magnetic energy of the microdroplets varies as the chain conformations

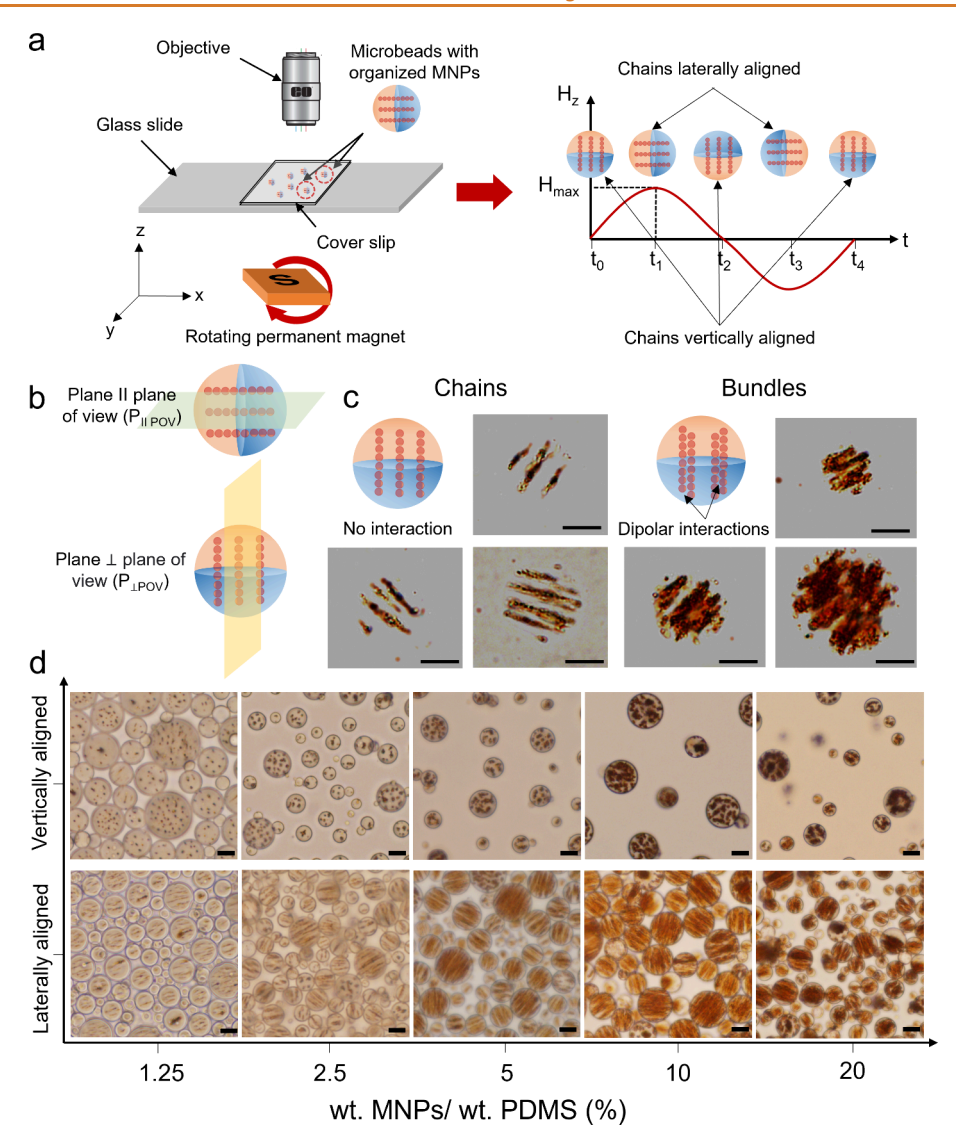


Figure 2. (a) Schematic of the orientation of the MD-DOMs in the vicinity of a permanent magnet rotating along the y-axis. The MNP structures assembled inside the MD-DOMs can be aligned laterally or vertically by creating a rotating magnetic field. (b) Direction of orientation of the chains as the microdroplets are rotated. The chains are oriented parallel to $P_{\parallel POV}$ and $P_{\perp POV}$ planes for lateral and vertical orientations, respectively. (c) Distinction between chains and bundles inside the droplets or microbeads. Optical images from RI-matched beads show that the chains are separated from each other, while in bundles, multiple chains are aggregated in thick formations. (d) Optical micrographs of MD-DOMs in vertical and lateral alignments at different MNP wt % illustrating the structural organization change from chains to bundles. The scale bar represents 10 μ m.

change within a microdroplet of a specific size under an applied field, corroborating our experimental findings. Finally, we cure these droplets to form microbeads and show how predicting the assembly behavior aids in the design of functional materials for applications such as optical modulation and active propulsion.

RESULTS AND DISCUSSION

Synthesis of Microbeads Containing Randomly Organized (MD-ROMs) and Directionally Oriented (MD-DOMs) MNPs. First, we discuss the making of a dispersion of PDMS liquid microdroplets without embedded nanoparticles (MDs) through impeller-induced fragmentation in shear thinning fluids (Figure 1a). Here, the liquid PDMS precursor and the curing agent were premixed in a bulk medium of 14 wt % poly(vinyl alcohol) (PVA). They were first emulsified at 150 rpm and then sheared at different impeller speeds ranging from 250 to 1000 rpm to form spherical PDMS microdroplets (Figure

S1). The wt % of PVA was chosen such that the viscosity of PVA nearly matches the one the PDMS precursor, which led to the formation of monodisperse droplets. ^{59,60} For the lower shearing speed of 250 rpm, we obtained a size distribution of 7.39 \pm 2.3 μ m, which narrowed down to 3.94 \pm 1.04 μ m when the impeller speed was increased to 1000 rpm (Figure S2). These droplets were finally cured at 60 °C to form the microbeads (MBs).

The synthesis of microbeads with embedded MNPs followed a similar procedure as discussed above except that we dispersed the iron-oxide nanoparticles in the PDMS liquid precursor medium before the shearing step. We first dispersed the MNPs in tetrahydrofuran (THF) and then added it to the PDMS precursor to achieve a uniform suspension of PDMS precursor with embedded MNPs (Figure 1b). Consequently, in the emulsification phase, we generated microdroplets containing MNPs. The MNP concentrations in the PDMS precursor were systematically varied from 1.25% to 20% (w/w). At this stage, in

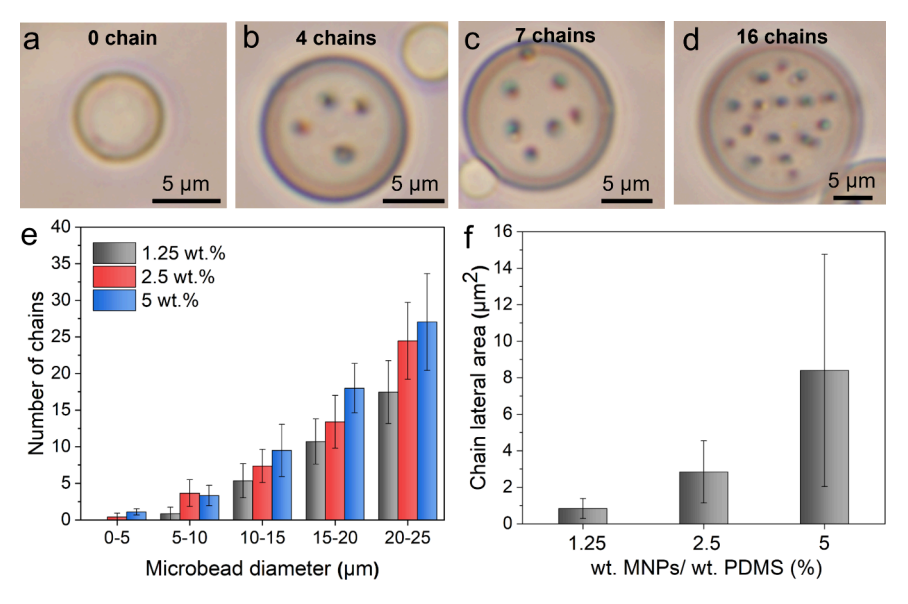


Figure 3. (a—d) Optical micrographs of MD-DOMS at 1.25 wt % MNPs with different number of chains at different diameters. (e) Bar plot of the number of chains vs microdroplet diameter at MNP wt % ranging from 1.25 to 5. (f) Average lateral area per chain vs MNPs wt % showing the increase in their cross-sectional thickness.

the absence of magnetic field, there is no preferential arrangement of the MNPs; they were randomly organized (ROMs) throughout the droplets. We refer to these microdroplets as MD-ROMs, which can be cured to form microbeads with randomly organized MNPs (MB-ROMs). A sequence of optical micrographs of the MB-ROMs for different MNP concentrations is presented in Figure S3, which shows that the nanoparticles exist in a state of micron-sized clusters, possibly formed as a result of their residual ferromagnetic interactions. Since we avoided the shearing of the droplets at different impeller speeds in this case, we attained a broad size distribution of the MB-ROMs ranging from 1 to 25 μ m for all MNP concentrations.

In the case of microdroplets with directionally oriented MNPs (MD-DOMs), we applied a static magnetic field of 15 mT before and during the curing step. The field is uniform at the scale of any individual droplet, although the intensity of the global magnetic field may vary slightly. This field organized the randomly distributed MNPs inside the droplets to form directionally aligned anisotropic structures during cross-linking, as seen in Figure 1c. It is important to note that the chains shown in the schematic are linear assemblies of micron scale nanoparticle clusters, rather than single nanoparticles.

Hierarchical Patterns of MNP Assemblies inside Microdroplets under Magnetic Field. We used PDMS microdroplets as our confined microgeometry model system and examined the organization of the magnetic architectures inside the MD-DOMs as we varied the concentration of the MNPs. The assemblies and the interactions between them were observed by rotating and aligning the MD-DOMs using a permanent magnet (Figure 2a). This caused the assemblies to transition their configuration from laterally aligned structures to vertically aligned structures. We refer to the former structures as being coplanar with any planes parallel to the plane of view of the microscope $(P_{\parallel POV})$, and the later ones as being coplanar with any planes perpendicular to the plane of view $(P_{\perp POV})$ (Figure 2b). By immersing the beads in refractive index (RI) matched silicone oil, we could visualize the cross-sectional structure of these assemblies along $P_{\perp POV}$ and could accurately distinguish

between chains and bundles (Figure 2c). As seen from these high magnification optical images, the thin chains are spaced far apart due to repulsive interactions, while in the case of bundles, the chains aggregate laterally during the assembly process.

We present a set of optical images in Figure 2d, showcasing the assemblies inside the droplets as a function of increasing MNP loading for two different configurations, i.e. when the chains are laterally aligned and when they are vertically aligned. At the lower MNP loading of 1.25%, the MNPs aligned tangential to the field, forming multiple short chains as evident from their lateral alignment images. Upon increasing the MNP concentration to 2.5%, they further formed long thick chains running from one to the other ends of the droplet. The chains were spaced far apart from each other, indicating the lack of lateral attraction between them. Similar short and long chains have been reported earlier by Liu et al. in their simulation study of dynamic magnetic assembly of paramagnetic particles in confined microspheres.⁶¹ An intermediate MNP loading of 5% led to lateral coalescence of the 2D chains normal to the field direction due to short-range attraction between neighboring chains. These chains then started to coarsen to form bundles. This transformation was most effectively visualized when the assemblies were reoriented along P_{LPOV}, revealing the emergence of large irregular cross sections in the assemblies due to chain aggregation. Yet, some 2D chains were still far away from each other, and did not fall within the capture radius of each other, i.e. the interchain separation is large enough such that the attractive interactions do not dominate to assemble them further. Subsequently, with increasing MNP concentrations reaching 10% and beyond, all of the chains eventually collapsed to form semicrystalline structures or thick bundles.

In the presence of a magnetic field \vec{H} , the MNPs acquire a magnetic moment $\vec{m_i} = V_i \vec{X} \vec{H}$, where V_i is the volume of magnetized domain, X is the effective magnetic susceptibility. The MNPs exhibit attractive dipolar interactions along the field direction, resulting in alignment even over long interparticle distances. Two dipoles separated by a distance of r_{ij} experience an interaction potential, which is given by

$$U_{ij} = \frac{\mu_0}{4\pi r_{ij}^3} \left[(\overrightarrow{m_i}. \overrightarrow{m_j}) - 3 \frac{(\overrightarrow{m_i}. \overrightarrow{r_{ij}})(\overrightarrow{m_j}. \overrightarrow{r_{ij}})}{r_{ij}^2} \right]$$
(1)

$$U_{ij} = \frac{\mu_0 V_i V_j X^2 \mathbf{H}^2}{4\pi r_{ij}^3} [1 - 3\cos\theta]$$
 (2)

where μ_0 is the vacuum permeability, \vec{r}_{ij} is the position vector between the dipoles and θ is the angle between the position vector and the magnetic field. At $\theta = 0^{\circ}$, the strength of the dipolar interactions at low MNP loadings (such as 1.25 and 2.5 wt %) is maximized, leading to assembly of linear MNP chains with a head-to-tail configuration among the particles. These chains laterally repel each other and stay as far as possible apart. Although the chains were fragmented in the case of 1.25 MNP wt %, the chain separation decreases with increasing MNP density such as 2.5% MNP loading. As a result, the short chains interacted to form long chains, which extend throughout the MD-DOMs. In bulk systems, the final equilibrium state of these assemblies is mostly determined by the particle concentration and the interactions between the MNPs. However, in droplets, the confinement represents a third factor, which affects the final states. The characteristic length of the chains inside the MD-DOMs is governed by their position inside the droplets. It is evident that the chains near the equatorial plane of MD-DOMs oriented along the field were longer than the ones far away from the equatorial plane. This is an interesting finding, which we do not generally see in bulk systems, where the particles form chains of uniform length. Second, because of confinement, the chains are not allowed to grow indefinitely, as in bulk systems. Instead, the chains separate out across multiple planes coplanar with the field along z directions inside the microdroplets. Third, at high MNP concentrations of 5 to 20%, in spite of very strong lateral interchain repulsion, the chains could not separate as far as possible to minimize their energy since they are confined inside the droplets. Thus, the system reaches a magnetostatically unstable state.²³ An attractive short-range potential exists between flexible chains that seems to coarsen the system to form 3D bundles.^{20,21}

Next, we counted the number of chains inside the MD-DOMs of increasing sizes at MNP concentrations from 1.25% to 5% (Figure 3a-d and Figure S4). It is evident that the number of chains was strongly correlated to the droplet size, irrespective of the MNP concentration (Figure 3e). For MD-DOMs larger than 10 μ m, we also see that the number of chains increased with increasing MNP concentration. We further fitted the scatter plots with curves to evaluate how the number of chains (n_{chains}) varied as a function of the PDMS microdroplet diameter, $d_{MD-DOMs}$ (Figure S5). It was found that the number of chains followed a power-law scaling relationship, i.e., $n_{chains} \sim$ $(d_{MD-DOMs})^z$. The scaling exponent z was ≈ 2 , which confirmed that the number of chains increased linearly with respect to the microdroplet cross-sectional area. The density of chains per unit area of the microdroplets remained constant and thus helped us to accurately predict the number of chains inside MD-HOM of a fixed size. Overall, $n_{chains} \sim (d_{MD-DOMs})^2 \times concentration_{MNP}$. Finally, we plotted the average lateral area per chain (Figure 3f), which was determined from the cross-sectional area of the chains as they face along $P_{\perp POV}$. The lateral area was found to increase from $0.83 \, \mu\text{m}^2$ to $8.39 \, \mu\text{m}^2$ as the MNP concentration increased from 1.25% to 5%. The increase in the cross-sectional area of the chains validated the evolution of hierarchical structures from

thin chains to thick chains to coexistence of chains and bundles as we vary the MNP concentration from 1.25% to 5%.

An overall state diagram summarizing the phase transition of the microstructures across various diameters of MD-DOMs and different MNP loadings is presented in Figure 4. We have

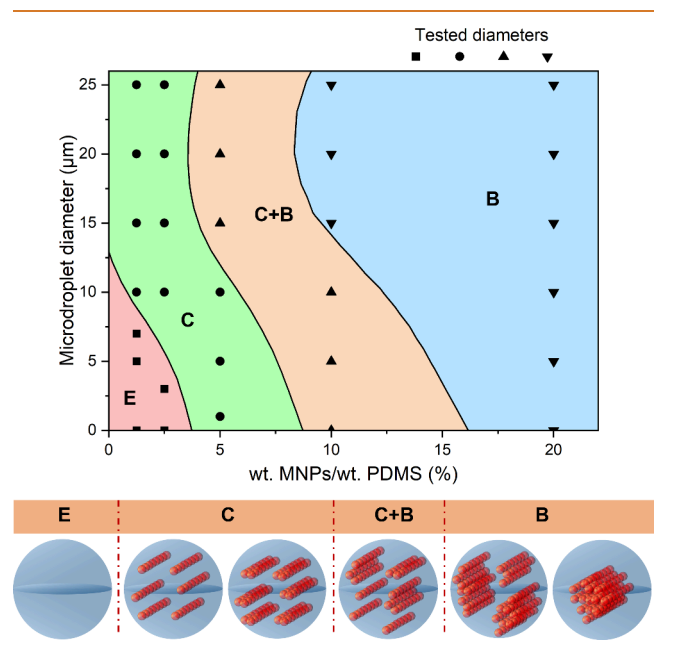


Figure 4. Microstructural state diagram of the organization of the hierarchical assemblies inside MD-DOMs of different diameters at MNPs wt % ranging from 1.25% to 20%. The system marked as E corresponds to randomly dispersed particles or empty beads, C corresponds to chains only, C+B corresponds to chains + bundles, B corresponds to bundles only (schematic not to scale).

identified 4 distinct phases: uniform dispersion or empty beads (red), only chains (green), chains coexisting with bundles (orange) and only bundles (blue). Below a threshold diameter of MD-DOMs (0–4 μ m) and concentration of MNPs (0–8 wt %), chain formation is absent. From eq 2, it is evident that $U_{\min} \propto \frac{V_i V_j}{r_{ij}^3}$, when $\theta = 0^\circ$. The interparticle distance at which this magnetic energy is equal to the thermal energy is known as the capture radius R_c and is given by

$$R_c \propto \left(\frac{V_i V_j}{T}\right)^{1/3} \tag{3}$$

The second important length scale that governs the magnetic assembly is the initial average interparticle spacing of the randomly distributed MNPs in the droplet prior to field exposure, which is given by $R_0 \propto (\Phi_i \Phi_j)^{-1/3}$, where Φ represents the volume packing fraction of the magnetic domain. 62 If R_c/R_0 < 1, the thermal fluctuations dominate over the magnetic interactions and the assembly is diffusion-limited, i.e. the MNP must diffuse into the capture radius to form chains. This typically happens in smaller droplets with low MNP loading. However, due to high viscous drag of the PDMS precursor, the diffusion kinetics is much slower than the time scale of curing, which inhibits chain formation. As a result, they displayed a gas-like behavior. However, as both the microbead diameter and MNP wt % increased, R_c/R_0 becomes >1 and the magnetic energy dominates over thermal fluctuations. MNPs instantaneously start forming chains or string fluids parallel to the field

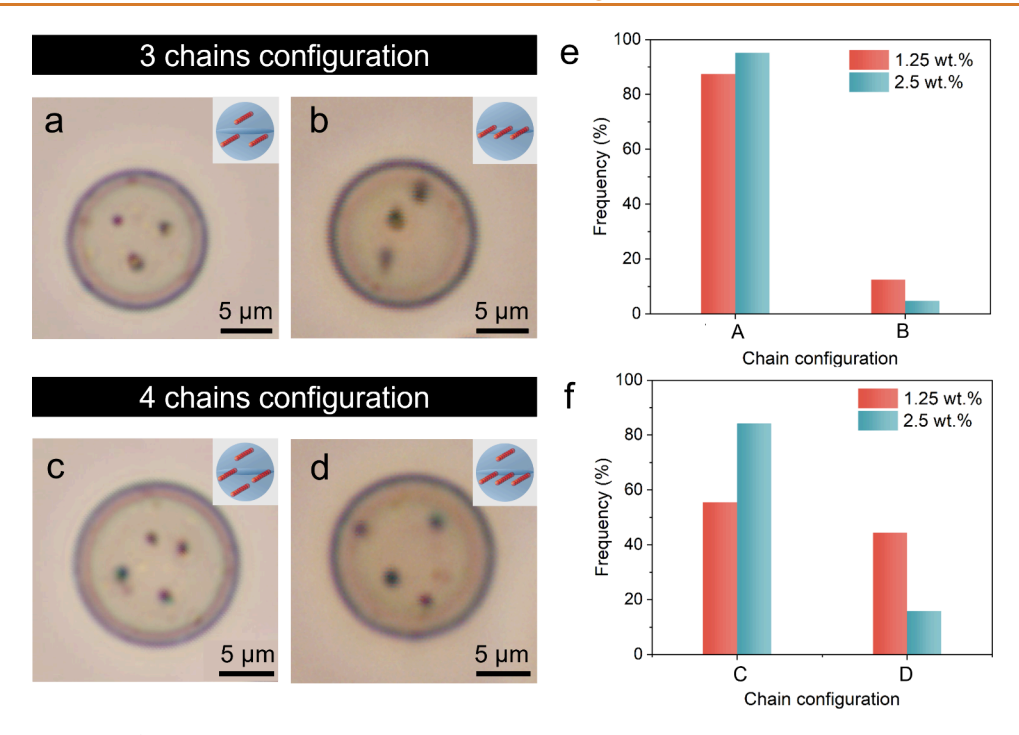


Figure 5. (a-d) Arrangement of the microstructures within MD-DOMs at a 1.25 wt % MNP loading when the chains are aligned vertically along $P_{\perp POV}$ plane. Configurations a and c represent the preferred out-of-plane triangular and quadrilateral arrangements, whereas configurations b and d are the less favorable. The insets provide 3D schematic representations of these chain configurations within confined spaces. (e and f) Frequency of observing various configurations based on experimental data from 3 chains and 4 chains systems, respectively.

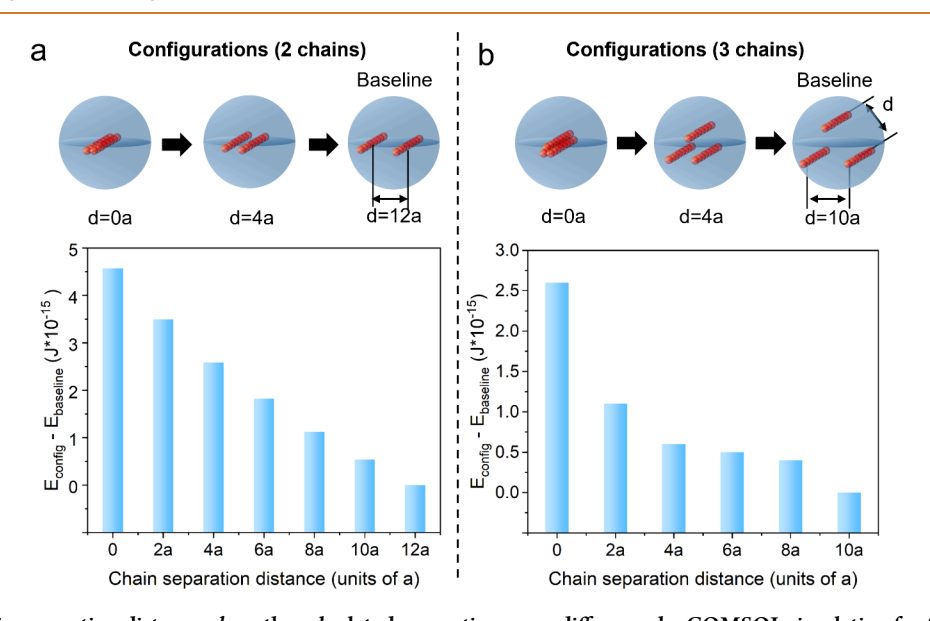


Figure 6. Effect of chain separation distance, d, on the calculated magnetic energy difference by COMSOL simulation for (a) two chains and (b) three chains inside MD-DOMs. The chain separation distance is presented in multiples of 2a (a is the MNP radius).

direction.⁶³ Hynninen and Dijkstra reported similar types of structures of colloidal dipolar hard spheres in an infinite domain by simulation at low particle densities oriented by external fields.⁶⁴ As depicted by the schematic in Figure 4, there can be either thin chains or thick chains which consist of multiple MNPs.

A phase transition from only chains to coexistence of both chains and bundles is observed at MNP weight percentages as low as 4% for MD-DOMs with sizes ranging from 15 to 25 μ m, and as high as 16% for MD-DOMs with a size of 1 μ m. This is equivalent to the hard sphere phase behavior with a dipole moment where the system shows a first-order phase transition

from fluid phase (chains) at low MNP volume fraction to face-centered-cubic solid (bundles) at high volume fraction. ^{65,66} At MNP wt $\% \ge 9$, the packing fraction of the body-centered-tetragonal phase keeps on increasing as the chains vanish entirely, and the assemblies consist solely of bundles. This region broadens at high MNP concentrations where the nanoparticles have less mobility and are unable to relax to their lowest energy because of high lateral repulsion between the chains. Therefore, the MNP chains collapse on each other out of registry by overcoming the energy barrier forming bundles with "zipped" chains.

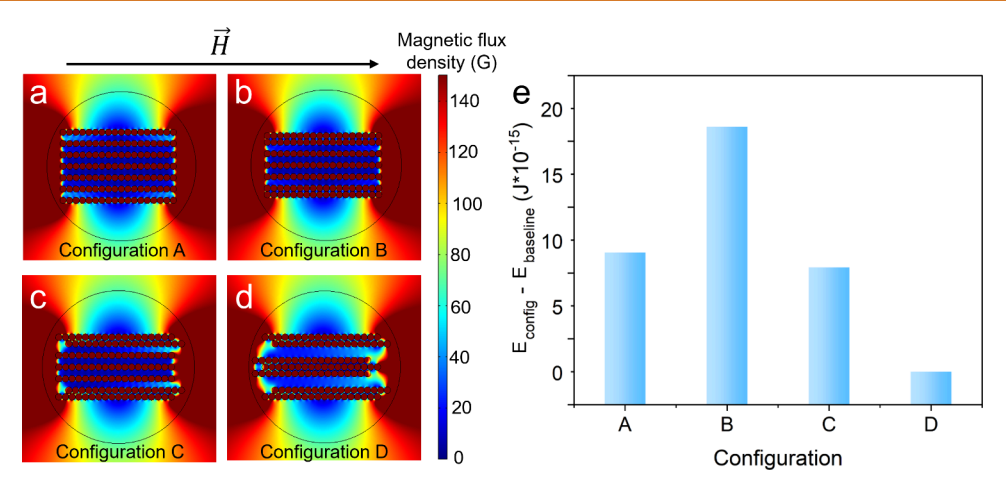


Figure 7. (a-d) Simulations of the magnetic flux density for different configurations ranging from individual chains to bundles inside MD-DOMs at higher MNP loading. The bar to the right of a-d indicates the magnetic flux intensity (in G). (e) The effect of chain configuration on the magnetic energy difference.

We further explored the orientation of the microstructures inside the MD-DOMs under conditions of very low chain densities such as MNPs forming 3 or 4 chains (Figure 5a-d and Figure S6). This offers an insight into how the structural characteristics of the magnetic assemblies differ in confined microgeometries compared to unconfined systems. Two types of configurations were observed in the 3 chains system: 1) the chains aligned such that they formed an out-of-plane triangular configuration, and 2) they aligned on the same plane. The frequency of the chains with out-of-plane alignment observed experimentally from 30 droplets is roughly 7× higher than the frequency of coplanar conformation for 1.25 MNP wt % and 20× higher for 2.5 wt % (Figure 5e). This finding showed that the out-of-plane triangular configuration of the chains is a more stable state as opposed to their in-plane configuration. The former permits larger distance of separation between the three chains than their in-plane configuration in a confined geometry of a fixed area and minimized the overall potential energy. Similarly, in a 4 chains system, they aligned in a quadrilateral pattern (Figure 5f), which is the preferable arrangement of fitting a fourth chain in the confined space with chain repulsion. We do not see this unconventional chain arrangement in unconfined geometries, where in fact the opposite holds true, i.e. the chains mostly arrange in the same plane, parallel to the field. Therefore, our results confirmed that the spatial confinement of the host droplets plays a role in the arrangement of the MNP microstructures during the assembly.

Modeling of MNP Assembly in Confined Microgeometries. To evaluate the effect of MNP concentration on the microstructural phase transition, we performed 2D and 3D finite element analysis of the magnetic field distribution in systems with chains with MNPs of radius *a* confined in a PDMS microdroplet under a static magnetic field of 15 mT. Here, we followed a "quasi-Monte Carlo" approach where the position of the chains was changed to simulate and compare the different types of structures that could form inside the MD-DOMs at various MNPs weight fractions. 32,67 The total magnetic energy stored in the system was calculated. This procedure was repeated until we identified the configuration with minimum stored magnetic energy, which corresponds to the most favorable chain arrangement.

For low MNP concentration, we simulated MD-DOMs systems containing 2 chains (Figure 6a) and 3 chains (Figure

6b). For the 2-chain system, the configuration with the chains at a separation distance (d) of 12a is considered as the baseline. It corresponds to the largest separation distance possible, as the chains cannot move further because of the microdroplet confinement. This base assembly was compared with other configurations where we decreased the chain separation distance by 2a, until they were aligned laterally to each other. The simulation of the magnetic flux density (Figure S7) showed that the magnetic energy was lower in the case of maximal separation of the chains and that the energy difference increased as we decreased the interchain separation. Similarly, for the 3-chain MD-DOMs, the equilibrium configuration was an equilateral triangle in good correspondence of what was found in the experimental observations. In this case, the magnetic energy also decreased with an increase in the interchain separation distance from 0 to 10a, thereby confirming the triangular configuration of chains as the favorable one.

Four configurations were examined for the case of modeling of systems at higher MNP loading where we saw bundle formation in our experiments (Figure 7a-d). In configuration A, the chains were evenly spaced, while in the remaining configurations, the chains started interacting laterally and formed bundles. Both configurations B and C had two pairs of chains at the top and bottom forming bundles. In configuration B, the MNP dipoles in each of these bundles were in registry, i.e. the center of the MNP in one chain was aligned with the center of the MNP of the other chain in the bundle. In configuration C, the chains had offset dipoles or out of registry, i.e. the second chain is shifted by 3a with respect to the other. Finally for configuration D, all chains collapsed laterally to form three bundles. As anticipated, our simulation showed that although the energy increases as the chains with induced dipoles aggregate laterally, it drops when the dipoles are organized in the more favorable out-of-registry configuration (Figure 7e). The energy decreased further as more out-of-registry chains formed bundles. For reference, we also simulated a microdroplet with the same number of randomly dispersed MNPs (Figure S8). It was found to have an (unfavorable) energy difference of 1.42×10^{-13} J with respect to the baseline chained configuration. This difference is nearly 600× higher than the energy difference of configuration B with respect to the baseline, which confirms our hypothesis that the bundles are the dominant configurations at higher MNP loading. Theoretical calculations had shown previously that

there is a critical length of the chains above which the formation of bundles with chains in zipped configuration is energetically favorable. The calculated critical length depends on the number of particles in the chains, and is typically >14. This happens because the decrease in magnetic energy for head-to-tail alignment of longer chains saturates at $-1.64\ U_{\rm min}\ (U_{\rm min}$ is the minimum magnetic energy). Therefore, at high MNP loading inside the droplets, the chains form bundles in zipped configuration through short-range attraction at the expense of long-range repulsion.

Magnetic Properties of MB-ROMs and MB-DOMs. The magnetization (M) of the microbeads with randomly organized (MB-ROMs) and directionally oriented (MB-DOMs) MNPs were measured at 300 K as we scanned the magnetic field (H) between ± 50 kOe (Figure 8). Diamagnetic contributions of the

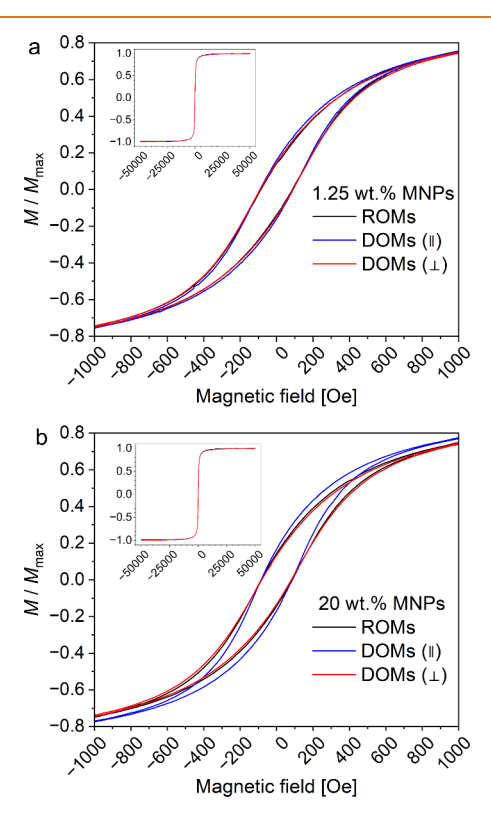


Figure 8. Field-dependent magnetization for MB-ROMs and MB-DOMs measured parallel and perpendicular to the direction of the MNP assemblies at 300 K: $(\pm 1000 \text{ Oe})$ (a) 1.25 wt % and (b) 20 wt %. Insets show the full magnetization curves.

PDMS polymer and sample holder were removed by adding a linear magnetization with an intercept at the origin to the magnetization curve, forcing the curves to saturate to a flat line. These curves were then normalized with respect to the maximum magnetization (M_{max}) to make $|M| \leq 1$ because the low mass of MNPs in each sample is difficult to measure and would result in significant uncertainties in an absolute magnetization scale. The magnetization of the MB-ROMs and MB-DOMs was found to be consistent with those of the MNPs (Figure S9). Chaining had a minor effect on the steepness of the magnetization curves corresponding to the difference in the magnetization along the chain direction and perpendicular to the chain direction.

For both the 1.25 and 20 wt % MD-DOMs, the parallel orientation of the assemblies has the easiest magnetization, and

the perpendicular orientation has the hardest magnetization, i.e. the parallel orientation had a steeper slope in the M vs H curve as compared to the perpendicular orientation. For reference, we also characterized the MB-ROMs, which had an intermediate magnetization that is somewhat closer to the perpendicular curve than the parallel curve. These differences are reflected in the remanent magnetization (M_{rem}) when H is equal to 0 Oe. But the coercivity or the magnetic field required to demagnetize the microbeads (see H at |M| = 0) is not affected by chaining, which is consistent with previous studies of chained MNPs. 14 Among all measurements, the coercivity ranges between 80 and 90 Oe, which is relatively low and consistent with MNPs that are ferromagnetic at room temperature, but are strongly affected by thermal energy and are nearly superparamagnetic. These results are consistent with expectations for the chains to impart magnetic anisotropy, such that magnetization parallel to the chains is favorable and perpendicular to the chains is unfavorable. In principle, the differences in the magnetization curves can be related to the magnetic torque exerted on the chain, but we are not aware of straightforward models for establishing this relationship.

Applications of MB-DOMs Based on Field-Induced Torque. Now, we discuss how the macroscopic magnetic response of the cured microbeads (MBs) depends on the MNP structuring inside them. Our results allow us to distinguish 4 different systems where the response of the beads differs based on the structuring of the embedded MNPs and their magnetic polarizability. Magnetic particles that are homogeneously distributed throughout the MB-ROMs have weak polarizability and do not respond to torques under continuously rotating fields (Figure 9). However, the anisotropic organization of the MNPs inside MB-DOMs leads to a strong magnetic polarization in the direction of the chains as shown from the magnetometry results. If the MB-DOMs are subjected to a rotating magnetic field, they will exhibit torque due to the tangential component of the dipolar force and will align with the field. This field-induced torque of the microbeads will subject them to rotate in-plane or out-of-plane depending on the rotation direction. Video S1 shows how our MB-DOMs rotate in place in dilute suspensions upon applying an in-plane rotating field.

If the MNPs embedded inside the MBs are superparamagnetic, the MNP chains will lose memory of their previous polarization when the field is turned off, due to their negligible residual polarization. As a result, the microbead chains will disassemble via Brownian motion and can be reconfigured on-demand. In contrast, if the aligned MNPs have residual polarization such as iron oxide MNPs used in our study, they can remain macroscopically chained when the field is turned off. The magnetic permeability of the cured PDMS matrix is close to one of vacuum and can be safely ignored. Rather, the magnetic polarizability of the MNP assemblies embedded inside the microbeads governs the overall chaining behavior of the MB-DOMs. As seen in Figure 9, the MNP assemblies inside the microbead face head-to-tail in dipolar interaction with other microbeads. Further investigations are needed to understand the dynamic arrangements of the bead assemblies in concentrated systems in response to different types of magnetic fields.

Overall, the 4 types of MB systems synthesized here by combining different types of MNP structures inside the microbeads along with various remanent magnetization profiles provide an "interactions toolbox" for these soft micro magnets. Based on the applications needed, this toolbox can be used to adjust the required response, dynamics, and structuration of the

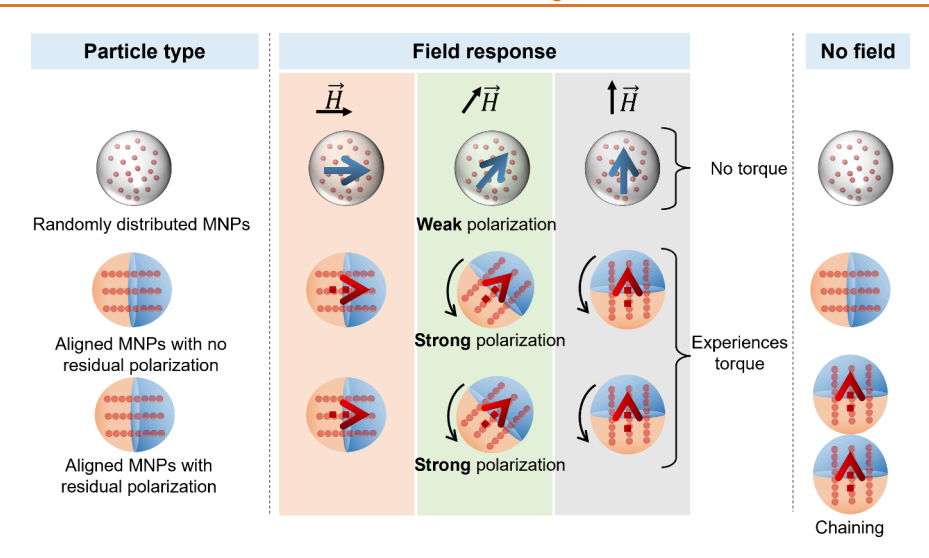


Figure 9. General behavior of cured MB-ROMs and MB-DOMs in rotating magnetic fields. MB-ROMs do not experience any torque, while the MB-DOMs experience torque and align dynamically with the rotating field. MB-DOMs can be further redispersed or can remain assembled into chain-like structures when the rotating magnetic field is switched off depending on the residual polarization of the embedded MNPs structures.

MB system. In the next section, we describe how we take advantage of the torque-induced rotation of the MB-DOMs to demonstrate two types of potential applications: (i) active microrollers and (ii) systems with optical modulation of the transmitted light.

Magnetically Actuated Micro Rotors. Our MB-DOMs have excellent magnetic responsiveness, and, as a result can serve as magnetically actuated microrollers. One common method to propel a magnetic microroller is by actuating it with a magnetic field in the plane perpendicular to a surface or a wall, which breaks the flow-field symmetry around the particle. ^{70–72} As a result, the rotating spherical particle experiences different hydrodynamic resistances at the bottom and the top, resulting in translational motion. ⁷³ The MB-ROMs and MB-DOMs dispersed in DI water were subjected to a circularly polarized rotating magnetic field by a permanent magnet in the x-z plane, characterized by $\vec{H}(t) = H[\cos{(\omega t)}e_x - \sin{(\omega t)}e_z]$, where ω is the angular frequency of the magnetic field, t is the time and e_x and e_z represent the unit vectors along x and z axes (Figure 10a).

Notably, the nonstructured MB-ROMs were not able to respond to the magnetic torque created due to the rotating field and were not able to tumble in any direction (Figure 10b,e). On the other hand, MB-DOMs, with the chains continuously trying to align with the field, rotated due to a magnetic torque equal to $T_m = \mu_0(m^*H)$ where m is the magnetic moment of the microbeads. By rotating the permanent magnet clockwise or anticlockwise we generated clockwise or anticlockwise rotation of the microbeads (Figure 10c,d). The MB-DOMs roll along the substrate on top of the lubrication layer between the MB-DOMs and the substrate, 71,72 and can tumble forward (Video S2) or backward depending on the direction of rotation as shown in Figure 10f and g respectively. The dynamics of the microbeads is dictated by the balance between the magnetic torque (T_m) and viscous torque, $T_v = -\alpha_r \Omega$ where α_r is the rotational friction coefficient and Ω is the angular velocity of the microbead.⁷⁴ By tracking the displacement of the MB-DOMs (Figure 10h), we found that they could propel at a linear speed of 200 μ m/min at a magnetic rotational frequency of 35 rpm. The speed of the MB-DOMs was linearly proportional to the rotational frequency of the field and these rollers can have applications such as efficient

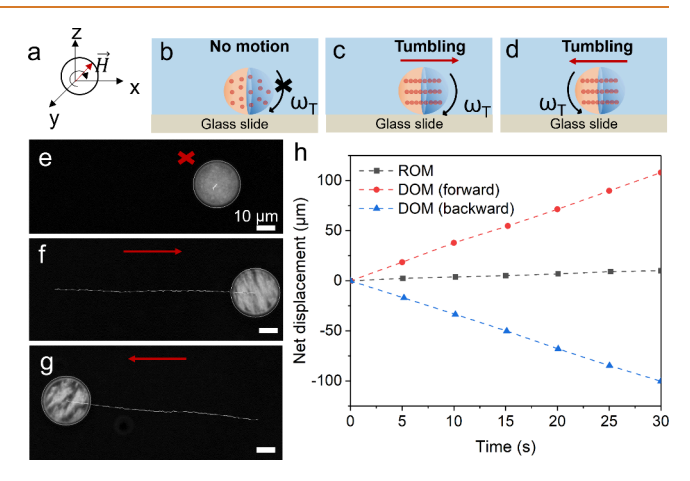


Figure 10. (a) Rotating magnetic field along x-z plane acting on different classes of microbeads. (b) No directional motion in the case of MB-ROMs, (c) forward propulsion and (d) backward propulsion of MB-DOMs due to clockwise and anticlockwise tumbling, respectively, in the presence of a rotating magnetic field. (e-g) Particle tracking of a 25 μ m microbead for 30 s showing no propulsion (MB-ROMs) vs forward/backward propulsion (MB-DOMs). h) Net displacement vs time graph.

microscale mixers or as microbots in biomedical and drug delivery.

Magnetically Responsive Optical Modulation. The anisotropic structure of the MB-DOMs could be used to control the transmission of the light through the microbeads when the orientation of the chain assemblies inside them is changed in relation to incident light. DDMS exhibits high transparency to visible light, and the light attenuation is entirely dependent on the nanoparticle structures in the beads. The uniformly distributed MNPs in MB-ROMs absorb incident light regardless of their orientation. They are also unresponsive to rotating fields and therefore lack optical modulation. In contrast, MB-DOMs enable localized optical modulation and macroscopic visual changes by adjusting chain orientation using a rotating magnetic field relative to the light source.

Figure 11a,b illustrates how when incident light is perpendicular to the magnetic field, laterally aligned chain

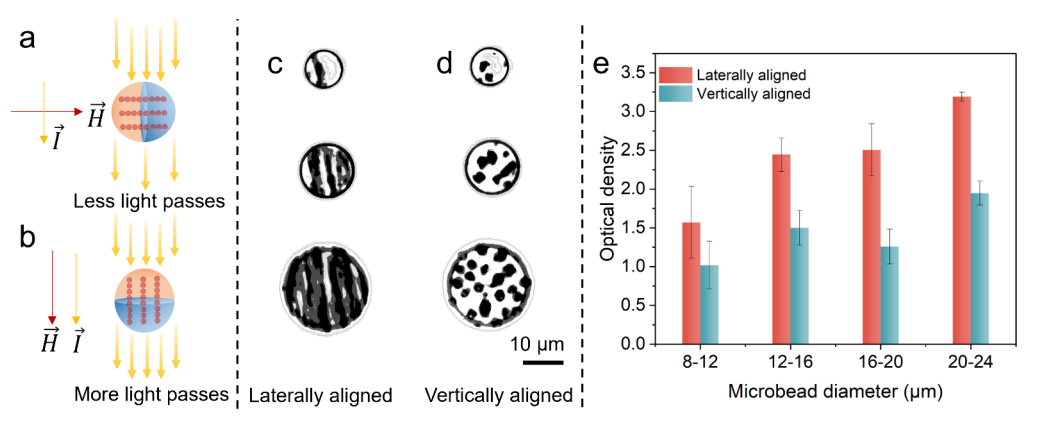


Figure 11. (a and b) Optical transmission of incident light when the magnetic field is perpendicular or parallel to the incident light causing the MB-DOMs to rotate from laterally aligned chains to vertically aligned chains. (c and d) Grayscale images of laterally aligned and vertically aligned MB-DOMs of different sizes at 2.5 wt % MNP loading. (e) Optical density variation between laterally aligned and vertically aligned MB-DOMs of different sizes.

assemblies have a high adsorbing cross-section, reducing light transmission. Conversely, parallel alignment of incident light and magnetic field allows more light to pass through the microbeads, since the chains are aligned normal to the plane of view (POV) and occupy less cross-sectional area inside the microbeads. It is noteworthy that we must choose a suitable MNP loading in which the longitudinal dimensions of the chain assemblies will be greater than their lateral dimensions. Therefore, we have chosen MB-DOMs with 2.5 wt % MNP loading, where the MNP chains have much larger characteristic length in one direction as compared to the other. As shown in grayscale images of such MB-DOMs with varying sizes (Figure 11c,d), the greater surface coverage by chains within microbeads indicate less transmission of light when the chains are aligned laterally. As the beads are rotated and the chains are realigned from $P_{\parallel POV}$ plane (perpendicular to incident light) to $P_{\perp POV}$ plane (parallel to incident light), we see an increase in white pixel intensity (Figure S10). The laterally aligned MB-DOMs exhibit approximately 60% higher optical density than vertically aligned ones (Figure 11e). Thus, our findings demonstrate that the optical density of these microbeads can be modulated through simple rotation under an external field.

CONCLUSIONS

We show that a static magnetic field can be used to create hierarchical structures by assembling magnetic nanoparticles confined inside microdroplets. At low MNP concentrations, chains of various lengths are formed, which coalesce at high MNP loading to form bundles with zipped chains by overcoming lateral repulsion. The formation of bundles is attributed to the confinement of the particles inside the droplets, where the assembled particle chains cannot grow to lengths comparable to the ones in bulk systems. The number of chains varies linearly with the bead cross-section area, while the cross-section of the assemblies increases with the nanoparticle concentration. We also observed out-of-plane geometrically stable arrangements such as triangular or quadrilateral patterns, which one does not intuitively expect to see in infinite domains. COMSOL simulations of the magnetic energy of various MNP structures show good agreement with the configurations that were found in the experimental studies. We show how four classes of particles with different magnetic response, polarizability and interactions can be formed after the assembled chains are immobilized in the cured PDMS droplets. These microbeads represent an

"interaction toolbox" with different dynamic responses and types of macroscale assemblies formed. We show how such functional microbeads with torque driven response can be used in systems with active roller propulsion and optical modulation. These four types of soft microbeads can be easily synthesized in scalable processes based on bulk emulsions. The possibility to fabricate such soft magnetic particles on a large scale could enable future applications such as biomedical formulations, drug delivery techniques, optical filters, smart windows, and sensors.

EXPERIMENTAL SECTION

Synthesis of Microbeads without and with Internally Embedded MNPs. In order to synthesize PDMS microbeads without internalized MNPs, first 14% poly(vinyl alcohol) (PVA) solution was prepared by adding 16.28 g of PVA (Mowiol 18-88, Sigma-Aldrich) to 100 mL of deionized water and was heated at 120 °C for 3 h under vigorous stirring at 400 rpm. Five g of PDMS precursor (Sylgard 184, Dow chemical) was mixed with the curing agent in the ratio of 10:1, degassed under vacuum and then added in 25 g of prepared 14% PVA solution. The emulsion was presheared using a Servodyne electronic mixer (Cole-Parmer, Model # 50003, USA) equipped with an impeller (three blades at 1 cm) at a shearing rate of 150 rpm for 15 min, leading to the formation of large, polydisperse silicone droplets. The droplets were further fragmented at various shearing rates of 250, 500, 750, and 1000 rpm for 30 min to synthesize PDMS microdroplets of higher monodispersity. Finally, the droplets were cross-linked at 60 °C for 5 h to synthesize the PDMS microbeads. The cured microbeads were centrifuged while washed with 0.1 wt % Tween-20 solution at 4400 rpm for 5 min to remove PVA from the suspension. This process was repeated five times, and the microbeads were finally dispersed in Tween-20 solution.

The making of MB-ROMs and MB-DOMs involved an initial step of dispersing the iron-oxide (Fe₂O₃) nanoparticles (50 nm, MKNano) in the PDMS precursor before emulsification. Calculated weights of MNPs for different wt % ranging from 1.25 wt % to 20 wt % were dispersed in tetrahydrofuran (THF) by ultrasonication using a probesonicator for 30 min. Notably, the MNPs were dispersed in the form of small micron-scale clusters, due to the residual magnetic interactions. The silicone precursor was then added to the nanoemulsion and ultrasonicated for another 30 min. In this way, THF temporarily reduced the precursor's viscosity. Finally, THF was Rota evaporated overnight to uniformly distribute the MNPs in the PDMS precursor. To synthesize MD-ROMs, the microdroplets were formed using a similar procedure as described above by emulsifying the PDMS precursor containing MNPs. An external attractive static magnetic field (15 mT) was applied before and during the curing step to orient the MNPs inside the droplet matrix, which formed MD-DOMs and eventually MB-DOMs after curing.

Optical Characterization. The microdroplets/microbeads along with the internalized structures were visualized by a bright field microscope (BX-61 Olympus). A suspension of the microbeads was placed on a glass slide and was enclosed from the top with a coverslip. In the case of high magnification optical images of the assemblies, we matched the refractive index by resuspending the microbeads in PDMS precursor. Thus, the boundary of the droplets disappears, and we could visualize only the assemblies inside. The assemblies may be difficult to observe using optical microscopy as they align laterally in the absence of an applied field. More specifically, the formation of dense or bundled chains of MNPs might be hard to observe when examining a MD crosssection across a single x-y plane. In order to address the limitation, a rotating magnetic field with maximum field strength of 0.6 mT was applied by rotating a Neodymium (NdFeB) magnet (size $1'' \times 1'' \times$ 0.125") 10 cm below the glass slide. This enabled us to rotate the microbeads and reorient them such that the assemblies are aligned perpendicular to the plane of view of the microscope ($P_{\perp POV}$). The total number of chains was calculated by counting the number of chains inside the droplets when they are oriented perpendicularly. The crosssectional area of the chains inside the MD-DOMs was measured using ImageJ by fitting a polygon around the chains oriented in the vertical direction.

The optical density of the MB-DOMs with laterally aligned and vertically aligned magnetic chains at 2.5 MNP wt % was determined by using a similar rotating magnetic field as discussed above. Before and after applying the rotating magnetic field, grayscale images were captured at a manual exposure of 1/500 s and 200 ISO in all cases. Subsequently, the images were binarized using MATLAB, and the pixel intensities were converted to optical density values. A pixel intensity of 0 corresponded to an optical density of 3.6, while a pixel intensity of 255 corresponded to an optical density of 0.

COMSOL Simulation. The energy calculations were performed using 2D and 3D finite element analysis with the magnetic field module of COMSOL multi simulation package 4.2. The solution space was divided into 3 subdomains: water media, spherical PDMS microdroplet of radius 12 μ m, and chains with 50 nm spherical iron-oxide MNPs. Specifically, for 2D simulation, the geometry was specified as the crosssectional top view of the MD-DOMs. The physical property values for relative permeability (μ) for each of these subdomains were specified as water media ($\mu = 1 - \chi_m = 1 - 9.04 \times 10^{-6}$), PDMS ($\mu = 1 - 9.04 \times 10^{-6}$) 10^{-6}), and iron oxide MNPs ($\mu = 30000$) where $\chi_{\rm m}$ is the magnetic susceptibility. An arbitrary background magnetic flux density was applied to the system. After the boundary conditions within the experimental cell were specified, the solution space was triangulated into a conformational mesh and refined further. The solver was initiated to calculate the magnetic field intensity by solving the Maxwell energy equations. The local magnetic energy density, w_B , in vacuum is $w_B = \frac{1}{2} \frac{B^2}{\mu_0}$ where B is the magnetic field intensity and μ_0 is the permeability of free space $(4\pi \times 10^{-7} \text{ N/A}^2)$. The total magnetic energy W_{R} of the system was then calculated by integrating w_{R} over the subdomain volume (V): $W_B = \int_V w_B dV$.

In the case of 2D simulation, this function integrated the magnetic energy across the 2D area and was therefore transformed to a 3D energy (with effective units of J) by multiplying by the microbead's radius. The calculations were repeated with more refined mesh sizes until the mesh was small enough for the final calculated values to vary by less than 0.05%.

Magnetometry Measurements. Magnetic characterization of the MB-ROMs and MB-DOMs was performed with a Quantum Design MPMS 3 superconducting quantum interference device (SQUID) vibrating sample magnetometer at 300 K. The magnetic microbeads suspended in 0.1% Tween-20 solution were drop casted onto a glass coverslip and dried before characterization. For the MB-DOMs, we further applied a magnetic field of 100 mT during the drying step to align all the microbeads along a specific direction. The sample was placed on a quartz rod and inserted into the magnetometer. The magnetization of the microbeads was measured with a scanning magnetic field from 50 kOe to -50 kOe, then back to 50 kOe. The "parallel" samples were measured with the field direction parallel to the

axis of the MNP assemblies for both 1.25 and 20 wt % samples, and the "perpendicular" samples were measured with the field direction normal to the axis of the MNP assemblies. It is worth noting that the parallel and perpendicular measurements were comprised from the same drop-casted sample but were from different sections and were not the same piece measured sequentially.

Propulsion Studies. A 50- μ L aliquot of suspension of the MB-ROMS or MB-DOMs in DI water was placed on a glass slide and was enclosed with a hydrophobic spacer at the periphery and a coverslip from the top. A rotating magnetic field as discussed above was applied using a permanent magnet (size 1" × 1" × 0.125") 10 cm below the glass slide and the microbeads motion was recorded for 30 s using a bright field Olympus BX-61 optical microscope. Particle displacements were tracked using ImageJ and measured across time lapses.

ASSOCIATED CONTENT

Supporting Information

The Supporting Information is available free of charge at https://pubs.acs.org/doi/10.1021/acsnano.4c06285.

(Figure S1) Optical images of PDMS microbeads without magnetic nanoparticles; (Figure S2) size distribution of PDMS microbeads; (Figure S3) optical images of PDMS microbeads with randomly distributed nanoparticles; (Figure S4) optical images of microbeads, illustrating the number of chains inside the MD-DOMs of various sizes for different MNP loading; (Figure S5) power law fit of the number of chains vs MD-DOMs diameter at different MNP wt %; (Figure S6) optical micrographs showing favorable and unfavorable chain configurations inside MD-DOMs; (Figure S7) simulations of the magnetic flux density around two chains inside a microdroplet; (Figure S8) simulation of a reference state where MNPs are randomly distributed in the microdroplet; (Figure S9) field-dependent magnetization of bare MNPs; and (Figure S10) counts vs pixel intensity for measuring optical density of the magnetic microbeads when they are aligned laterally and perpendicularly to the incident light (PDF)

Rotation of MB-DOMs under an applied in-plane rotating magnetic field (Video S1) (MP4)

Rorward tumbling of MB-DOMs under an applied out-ofplane rotating magnetic field (Video S2) (MP4)

AUTHOR INFORMATION

Corresponding Author

Orlin D. Velev — Department of Chemical & Biomolecular Engineering, North Carolina State University, Raleigh, North Carolina 27695, United States; orcid.org/0000-0003-0473-8056; Email: odvelev@ncsu.edu

Authors

Abhirup Basu — Department of Chemical & Biomolecular Engineering, North Carolina State University, Raleigh, North Carolina 27695, United States; orcid.org/0000-0002-8111-2877

Matthew R. Clary — Department of Materials Science and Engineering, North Carolina State University, Raleigh, North Carolina 27695, United States; orcid.org/0000-0003-4330-7689

Joseph B. Tracy — Department of Materials Science and Engineering, North Carolina State University, Raleigh, North Carolina 27695, United States; orcid.org/0000-0002-3358-3703 Carol K. Hall – Department of Chemical & Biomolecular Engineering, North Carolina State University, Raleigh, North Carolina 27695, United States; orcid.org/0000-0002-7425-587X

Complete contact information is available at: https://pubs.acs.org/10.1021/acsnano.4c06285

Author Contributions

O.D.V., C.K.H., and A.B. conceived and designed the project. A.B. conducted the experiments under the supervision of O.D.V. M.R.C., and J.B.T. carried out the magnetization study experiments. A.B. analyzed the data, made the figures, and wrote the manuscript through contributions from all the authors. All authors have given approval to the final version of the manuscript.

Notes

The authors declare no competing financial interest.

ACKNOWLEDGMENTS

This work is supported by the National Science Foundation grants CBET-1935248 and partially DMR-2303581. We acknowledge use of the MPMS in the Department of Materials Science and Engineering at North Carolina State University.

ABBREVIATIONS

PDMS:polydimethylsiloxane MNPs:magnetic nanoparticles MD:microdroplets with no na

MD:microdroplets with no nanoparticles inside MB:microbeads with no nanoparticles inside

MD-ROMs:microdroplets with randomly organized MNPs MD-DOMs:microdroplets with directionally oriented MNPs MB-ROMs:microbeads with randomly organized MNPs

MB-DOMs:microbeads with directionally oriented MNPs $P_{\parallel POV}$:plane parallel to the plane of view through the microscope

 $P_{\mbox{\scriptsize LPOV}}\mbox{:plane}$ normal to the plane of view through the microscope

REFERENCES

- (1) Glotzer, S. C.; Solomon, M. J.; Kotov, N. A. Self-Assembly: From Nanoscale to Microscale Colloids. *AIChE J.* **2004**, *50* (12), 2978–2985.
- (2) Kalsin, A. M.; Fialkowski, M.; Paszewski, M.; Smoukov, S. K.; Bishop, K. J. M.; Grzybowski, B. A. Electrostatic Self-Assembly of Binary Nanoparticle Crystals with a Diamond-like Lattice. *Science* (80-.) **2006**, 312 (5772), 420–424.
- (3) Prevo, B. G.; Kuncicky, D. M.; Velev, O. D. Engineered Deposition of Coatings from Nano- and Micro-Particles: A Brief Review of Convective Assembly at High Volume Fraction. *Colloids Surfaces A Physicochem. Eng. Asp.* **2007**, *311* (1–3), 2–10.
- (4) Velev, O. D.; Denkov, N. D.; Kralchevsky, P. A.; Ivanov, I. B.; Yoshimura, H.; Nagayama, K. Mechanism of Formation of Two-Dimensional Crystals from Latex Particles on Substrata. *Prog. Colloid Polym. Sci.* **1993**, 93 (12), 366–367.
- (5) Ding, T.; Song, K.; Clays, K.; Tung, C. H. Fabrication of 3D Photonic Crystals of Ellipsoids: Convective Self-Assembly in Magnetic Field. *Adv. Mater.* **2009**, *21* (19), 1936–1940.
- (6) Lalatonne, Y.; Motte, L.; Russier, V.; Ngo, A. T.; Bonville, P.; Pileni, M. P. Mesoscopic Structures of Nanocrystals: Collective Magnetic Properties Due to the Alignment of Nanocrystals. *J. Phys. Chem. B* **2004**, *108* (6), 1848–1854.
- (7) Mueggenburg, K. E.; Lin, X. M.; Goldsmith, R. H.; Jaeger, H. M. Elastic Membranes of Close-Packed Nanoparticle Arrays. *Nat. Mater.* **2007**, *6* (9), 656–660.

- (8) Basu, A.; Okello, L. B.; Castellanos, N.; Roh, S.; Velev, O. D. Assembly and Manipulation of Responsive and Flexible Colloidal Structures by Magnetic and Capillary Interactions. *Soft Matter.* **2023**, 19, 2466–2485. The Royal Society of Chemistry April 5
- (9) Spatafora-Salazar, A.; Lobmeyer, D. M.; Cunha, L. H. P.; Joshi, K.; Biswal, S. L. Hierarchical Assemblies of Superparamagnetic Colloids in Time-Varying Magnetic Fields. *Soft Matter* **2021**, *17* (5), 1120–1155. (10) Tracy, J. B.; Crawford, T. M. Magnetic Field-Directed Self-
- (10) Tracy, J. B.; Crawford, T. M. Magnetic Field-Directed Self-Assembly of Magnetic Nanoparticles. MRS Bull. 2013, 38 (11), 915–920
- (11) Han, K.; Shields, C. W.; Diwakar, N. M.; Bharti, B.; López, G. P.; Velev, O. D. Sequence-Encoded Colloidal Origami and Microbot Assemblies from Patchy Magnetic Cubes. *Sci. Adv.* **2017**, 3 (8), 1–7.
- (12) Han, K.; Shields, C. W.; Velev, O. D. Engineering of Self-Propelling Microbots and Microdevices Powered by Magnetic and Electric Fields. *Adv. Funct. Mater.* **2018**, 28 (25), 1705953.
- (13) Al Harraq, A.; Lee, J. G.; Bharti, B. Magnetic Field–Driven Assembly and Reconfiguration of Multicomponent Supraparticles. *Sci. Adv.* **2020**, *6* (19), 5337–5345.
- (14) Mishra, S. R.; Dickey, M. D.; Velev, O. D.; Tracy, J. B. Selective and Directional Actuation of Elastomer Films Using Chained Magnetic Nanoparticles. *Nanoscale* **2016**, *8* (3), 1309–1313.
- (15) Wang, M.; He, L.; Yin, Y. Magnetic Field Guided Colloidal Assembly. *Mater. Today* **2013**, *16* (4), 110–116.
- (16) Erb, R. M.; Son, H. S.; Samanta, B.; Rotello, V. M.; Yellen, B. B. Magnetic Assembly of Colloidal Superstructures with Multipole Symmetry. *Nature* **2009**, 457 (7232), 999–1002.
- (17) Håkonsen, V.; Singh, G.; Normile, P. S.; De Toro, J. A.; Wahlström, E.; He, J.; Zhang, Z. Magnetically Enhanced Mechanical Stability and Super-Size Effects in Self-Assembled Superstructures of Nanocubes. *Adv. Funct. Mater.* **2019**, 29 (46), 1904825.
- (18) Myrovali, E.; Papadopoulos, K.; Iglesias, I.; Spasova, M.; Farle, M.; Wiedwald, U.; Angelakeris, M. Long-Range Ordering Effects in Magnetic Nanoparticles. *ACS Appl. Mater. Interfaces* **2021**, *13* (18), 21602–21612.
- (19) Mehdaoui, B.; Tan, R. P.; Meffre, A.; Carrey, J.; Lachaize, S.; Chaudret, B.; Respaud, M. Increase of Magnetic Hyperthermia Efficiency Due to Dipolar Interactions in Low-Anisotropy Magnetic Nanoparticles: Theoretical and Experimental Results. *Phys. Rev. B Condens. Matter Mater. Phys.* **2013**, 87 (17), No. 174419.
- (20) Furst, E. M.; Gast, A. P. Dynamics and Lateral Interactions of Dipolar Chains. *Phys. Rev. E Stat. Physics, Plasmas, Fluids, Relat. Interdiscip. Top.* **2000**, 62 (5), 6916–6925.
- (21) Laskar, J. M.; Philip, J.; Raj, B. Experimental Evidence for Reversible Zippering of Chains in Magnetic Nanofluids under External Magnetic Fields. *Phys. Rev. E Stat. Nonlinear, Soft Matter Phys.* **2009**, 80 (4), No. 041401.
- (22) Nagaoka, Y.; Morimoto, H.; Maekawa, T. Ordered Complex Structures Formed by Paramagnetic Particles via Self-Assembly under an Ac/Dc Combined Magnetic Field. *Langmuir* **2011**, 27 (15), 9160–9164
- (23) Malik, V.; Petukhov, A. V.; He, L.; Yin, Y.; Schmidt, M. Colloidal Crystallization and Structural Changes in Suspensions of Silica/Magnetite Core-Shell Nanoparticles. *Langmuir* **2012**, 28 (41), 14777—14783
- (24) He, L.; Hu, Y.; Kim, H.; Ge, J.; Kwon, S.; Yin, Y. Magnetic Assembly of Nonmagnetic Particles into Photonic Crystal Structures. *Nano Lett.* **2010**, *10* (11), 4708–4714.
- (25) Nie, Z.; Fava, D.; Kumacheva, E.; Zou, S.; Walker, G. C.; Rubinstein, M. Self-Assembly of Metal-Polymer Analogues of Amphiphilic Triblock Copolymers. *Nat. Mater.* **2007**, *6* (8), 609–614.
- (26) Chen, Q.; Yan, J.; Zhang, J.; Bae, S. C.; Granick, S. Janus and Multiblock Colloidal Particles. *Langmuir* **2012**, 28 (38), 13555–13561.
- (27) Glotzer, S. C.; Solomon, M. J. Anisotropy of Building Blocks and Their Assembly into Complex Structures. *Nat. Mater.* **2007**, *6* (8), 557–562
- (28) Yan, J.; Han, M.; Zhang, J.; Xu, C.; Luijten, E.; Granick, S. Reconfiguring Active Particles by Electrostatic Imbalance. *Nat. Mater.* **2016**, *15* (10), 1095–1099.

- (29) Swan, J. W.; Bauer, J. L.; Liu, Y.; Furst, E. M. Directed Colloidal Self-Assembly in Toggled Magnetic Fields. *Soft Matter* **2014**, *10* (8), 1102–1109.
- (30) Promislow, J. H. E.; Gast, A. P. Magnetorheological Fluid Structure in a Pulsed Magnetic Field. *Langmuir* **1996**, *12* (17), 4095–4102.
- (31) Swan, J. W.; Bauer, J. L.; Liu, Y.; Furst, E. M. Directed Colloidal Self-Assembly in Toggled Magnetic Fields. *Soft Matter* **2014**, *10* (8), 1102–1109.
- (32) Smoukov, S. K.; Gangwal, S.; Marquez, M.; Velev, O. D. Reconfigurable Responsive Structures Assembled from Magnetic Janus Particles. *Soft Matter* **2009**, *5* (6), 1285–1292.
- (33) Ge, J.; Lee, H.; He, L.; Kim, J.; Lu, Z.; Kim, H.; Goebl, J.; Kwon, S.; Yin, Y. Magnetochromatic Microspheres: Rotating Photonic Crystals. J. Am. Chem. Soc. 2009, 131 (43), 15687–15694.
- (34) Hu, Y.; He, L.; Yin, Y. Magnetically Responsive Photonic Nanochains. *Angew. Chemie Int. Ed.* **2011**, *50* (16), 3747–3750.
- (35) He, L.; Wang, M.; Ge, J.; Yin, Y. Magnetic Assembly Route to Colloidal Responsive Photonic Nanostructures. *Acc. Chem. Res.* **2012**, 45 (9), 1431–1440.
- (36) Huang, H. W.; Huang, T. Y.; Charilaou, M.; Lyttle, S.; Zhang, Q.; Pané, S.; Nelson, B. J. Investigation of Magnetotaxis of Reconfigurable Micro-Origami Swimmers with Competitive and Cooperative Anisotropy. *Adv. Funct. Mater.* **2018**, *28* (36), 1802110.
- (37) Liu, J. A. C.; Gillen, J. H.; Mishra, S. R.; Evans, B. A.; Tracy, J. B. Photothermally and Magnetically Controlled Reconfiguration of Polymer Composites for Soft Robotics. *Sci. Adv.* **2019**, *5* (8), No. eaaw2897.
- (38) Schmauch, M. M.; Mishra, S. R.; Evans, B. A.; Velev, O. D.; Tracy, J. B. Chained Iron Microparticles for Directionally Controlled Actuation of Soft Robots. *ACS Appl. Mater. Interfaces* **2017**, 9 (13), 11895–11901.
- (39) Duhr, P.; Meier, Y. A.; Damanpack, A.; Carpenter, J.; Studart, A. R.; Rafsanjani, A.; Demirörs, A. F. Kirigami Makes a Soft Magnetic Sheet Crawl. *Adv. Sci.* **2023**, *10* (25), 2301895.
- (40) Castellanos, N. I.; Bharti, B.; Velev, O. D. Field-Driven Reversible Alignment and Gelation of Magneto-Responsive Soft Anisotropic Microbeads. *J. Phys. Chem. B* **2021**, *125* (28), 7900–7910.
- (41) Wang, Z.; Wu, Y.; Wu, D.; Sun, D.; Lin, L. Soft Magnetic Composites for Highly Deformable Actuators by Four-Dimensional Electrohydrodynamic Printing. *Compos. Part B Eng.* **2022**, 231, No. 109596.
- (42) Tao, H. Q.; Yue, D. W.; Li, C. H. A Fast Self-Healing Magnetic Nanocomposite for Magnetic Actuators. *Macromol. Mater. Eng.* **2022**, 307 (2), 2100649.
- (43) Roh, S.; Okello, L. B.; Golbasi, N.; Hankwitz, J. P.; Liu, J. A. C.; Tracy, J. B.; Velev, O. D. 3D-Printed Silicone Soft Architectures with Programmed Magneto-Capillary Reconfiguration. *Adv. Mater. Technol.* **2019**, *4* (4), 1800528.
- (44) Yan, Y.; Song, C.; Shen, Z.; Zhu, Y.; Ni, X.; Wang, B.; Christiansen, M.; Stavrakis, S.; Lintuvuori, J.; Chen, B.; DeMello, A.; Schuerle, S. Programming Structural and Magnetic Anisotropy for Tailored Interaction and Control of Soft Microrobots. *Res. Sq.* 2023, 7.
- (45) Giltinan, J.; Sridhar, V.; Bozuyuk, U.; Sheehan, D.; Sitti, M. 3D Microprinting of Iron Platinum Nanoparticle-Based Magnetic Mobile Microrobots. *Adv. Intell. Syst.* **2021**, 3 (1), 2000204.
- (46) Ijaz, S.; Li, H.; Hoang, M. C.; Kim, C. S.; Bang, D.; Choi, E.; Park, J. O. Magnetically Actuated Miniature Walking Soft Robot Based on Chained Magnetic Microparticles-Embedded Elastomer. *Sensors Actuators, A Phys.* **2020**, *301*, No. 111707.
- (47) Fan, Q.; Li, Z.; Wu, C.; Yin, Y. Magnetically Induced Anisotropic Interaction in Colloidal Assembly. *Precis. Chem.* **2023**, *1* (5), 272–298.
- (48) Wang, M.; He, L.; Xu, W.; Wang, X.; Yin, Y. Magnetic Assembly and Field-Tuning of Ellipsoidal-Nanoparticle-Based Colloidal Photonic Crystals. *Angew. Chemie Int. Ed.* **2015**, *54* (24), 7077–7081.
- (49) Zhang, G.; Gao, J.; Qian, J.; Cai, D.; Zheng, K.; Yu, Z.; Wang, J.; Zhong, K.; Zhang, X.; Wu, Z. A Multifunctional Magnetic Composite Material as a Drug Delivery System and a Magnetic Resonance Contrast Agent. *Part. Syst. Charact.* **2014**, *31* (9), 976–984.

- (50) Wang, Y.; Boero, G.; Zhang, X.; Brugger, J. Thermal and PH Sensitive Composite Membrane for On-Demand Drug Delivery by Applying an Alternating Magnetic Field. *Adv. Mater. Interfaces* **2020**, 7 (17), 2000733.
- (51) Park, J.; Kadasala, N. R.; Abouelmagd, S. A.; Castanares, M. A.; Collins, D. S.; Wei, A.; Yeo, Y. Polymer-Iron Oxide Composite Nanoparticles for EPR-Independent Drug Delivery. *Biomaterials* **2016**, *101*, 285–295.
- (52) Fermigier, M.; Gast, A. P. Structure Evolution in a Paramagnetic Latex Suspension. *J. Colloid Interface Sci.* **1992**, *154* (2), 522–539.
- (53) Hilou, E.; Joshi, K.; Biswal, S. L. Characterizing the Spatiotemporal Evolution of Paramagnetic Colloids in Time-Varying Magnetic Fields with Minkowski Functionals. *Soft Matter* **2020**, *16* (38), 8799–8805.
- (54) Hou, C.; Gao, L.; Wang, Y.; Yan, L. T. Entropic Control of Nanoparticle Self-Assembly through Confinement. *Nanoscale Horizons* **2022**, 7 (9), 1016–1028.
- (55) Manoharan, V. N. Colloidal Matter: Packing, Geometry, and Entropy. *Science* **2015**, 349, 6251.
- (56) Liu, Z.; Guo, R.; Xu, G.; Huang, Z.; Yan, L. T. Entropy-Mediated Mechanical Response of the Interfacial Nanoparticle Patterning. *Nano Lett.* **2014**, *14* (12), 6910–6916.
- (57) Damasceno, P. F.; Engel, M.; Glotzer, S. C. Predictive Self-Assembly of Polyhedra into Complex Structures. *Science* (80-.) **2012**, 337 (6093), 453–457.
- (58) Harper, E. S.; van Anders, G.; Glotzer, S. C. The Entropic Bond in Colloidal Crystals. *Proc. Natl. Acad. Sci. U. S. A.* **2019**, *116* (34), 16703–16710.
- (59) Mabille, C.; Leal-Calderon, F.; Bibette, J.; Schmitt, V. Monodisperse Fragmentation in Emulsions: Mechanisms and Kinetics. *Europhys. Lett.* **2003**, *61* (5), 708–714.
- (60) Mabille, C.; Schmitt, V.; Gorria, P.; Leal Calderon, F.; Faye, V.; Deminière, B.; Bibette, J. Rheological and Shearing Conditions for the Preparation of Monodisperse Emulsions. *Langmuir* **2000**, *16* (2), 422–429.
- (61) Liu, D.; Maxey, M. R.; Karniadakis, G. E. Simulations of Dynamic Self-Assembly of Paramagnetic Microspheres in Confined Microgeometries. *J. Micromechanics Microengineering* **2005**, *15* (12), 2298–2308.
- (62) Melle, S.; Rubio, M. A.; Fuller, G. G. Time Scaling Regimes in Aggregation of Magnetic Dipolar Particles: Scattering Dichroism Results. *Phys. Rev. Lett.* **2001**, 87 (11), 115501–115504.
- (63) Schmidle, H.; Hall, C. K.; Velev, O. D.; Klapp, S. H. L. Phase Diagram of Two-Dimensional Systems of Dipole-like Colloids. *Soft Matter* **2012**, *8* (5), 1521–1531.
- (64) Hynninen, A. P.; Dijkstra, M. Phase Behavior of Dipolar Hard and Soft Spheres. *Phys. Rev. E Stat. Nonlinear, Soft Matter Phys.* **2005**, 72 (5), No. 051402.
- (65) Rutkowski, D. M.; Velev, O. D.; Klapp, S. H. L.; Hall, C. K. Simulation Study on the Structural Properties of Colloidal Particles with Offset Dipoles. *Soft Matter* **2017**, *13* (17), 3134–3146.
- (66) Goyal, A.; Hall, C. K.; Velev, O. D. Self-Assembly in Binary Mixtures of Dipolar Colloids: Molecular Dynamics Simulations. *J. Chem. Phys.* **2010**, *133* (6), 64511.
- (67) Gangwal, S.; Cayre, O. J.; Velev, O. D. Dielectrophoretic Assembly of Metallodielectric Janus Particles in AC Electric Fields. *Langmuir* **2008**, 24 (23), 13312–13320.
- (68) Faraudo, J.; Camacho, J. Cooperative Magnetophoresis of Superparamagnetic Colloids: Theoretical Aspects. *Colloid Polym. Sci.* **2010**, 288 (2), 207–215.
- (69) Faraudo, J.; Andreu, J. S.; Calero, C.; Camacho, J. Predicting the Self-Assembly of Superparamagnetic Colloids under Magnetic Fields. *Adv. Funct. Mater.* **2016**, *26* (22), 3837–3858.
- (70) Tierno, P.; Golestanian, R.; Pagonabarraga, I.; Sagués, F. Magnetically Actuated Colloidal Microswimmers. *J. Phys. Chem. B* **2008**, *112* (51), 16525–16528.
- (71) Tasci, T. O.; Herson, P. S.; Neeves, K. B.; Marr, D. W. M. Surface-Enabled Propulsion and Control of Colloidal Microwheels. *Nat. Commun.* **2016**, 7 (1), 1–6.

- (72) Gao, Y.; Sprinkle, B.; Springer, E.; Marr, D. W. M.; Wu, N. Rolling of Soft Microbots with Tunable Traction. *Sci. Adv.* **2023**, *9* (16), No. eadg0919.
- (73) Demirörs, A. F.; Stauffer, A.; Lauener, C.; Cossu, J.; Ramakrishna, S. N.; de Graaf, J.; Alcantara, C. C. J.; Pané, S.; Spencer, N.; Studart, A. R. Magnetic Propulsion of Colloidal Microrollers Controlled by Electrically Modulated Friction. *Soft Matter* **2021**, *17* (4), 1037–1047. (74) Tierno, P.; Snezhko, A. Transport and Assembly of Magnetic Surface Rotors**. *ChemNanoMat* **2021**, *7* (8), 881–893.
- (75) Mattich, I.; Sendra, J.; Galinski, H.; Isapour, G.; Demirörs, A. F.; Lattuada, M.; Schuerle, S.; Studart, A. R. Magnetic Manipulation of Superparamagnetic Colloids in Droplet-Based Optical Devices. *Adv. Opt. Mater.* **2023**, *11* (21), 2300734.
- (76) Martinček, I.; Turek, I.; Tarjányi, N. Effect of Boundary on Refractive Index of PDMS. Opt. Mater. Express 2014, 4 (10), 1997.